The detailed dynamics of the June–August Hadley Cell

Received: 26 July 2019 | Revised: 4 October 2019 | Accepted: 22 October 2019

DOI: 10.1002/qj.3702

Quarterly Journal of the Royal Meteorological Society RMetS

INVITED MANUSCRIPT

The detailed dynamics of the June–August Hadley Cell

B. J. Hoskins[1,2] | G.-Y. Yang[1,3] | R. M. Fonseca[4,5]

[1]Department of Meteorology, University of Reading, Reading, UK

[2]Grantham Institute—Climate Change and the environment, Imperial College, London, UK

[3]Climate Directorate, National Centre for Atmospheric Science, University of Reading, Reading, UK

[4]Khalifa University of Science and Technology, Abu Dhabi, United Arab Emirates

[5]Division of Space Technology, Department of Computer Science, Electrical and Space Engineering, Luleå University of Technology, Luleå, Sweden

Correspondence
Gui-Ying Yang , NCAS Climate, Department of Meteorology,University of Reading, Earley Gate, Reading RG6 6BB
Email: g.y.yang@reading.ac.uk

Funding information
Natural Environment Research Council, R8/H12/83/007

Abstract

The seminal theory for the Hadley Cells has demonstrated that their existence is necessary for the reduction of tropical temperature gradients to a value such that the implied zonal winds are realisable. At the heart of the theory is the notion of angular momentum conservation in the upper branch of the Hadley Cells. Eddy mixing associated with extratropical systems is invoked to give continuity at the edge of the Hadley Cell and to reduce the subtropical jet by a factor of three or more to those observed. In this article a detailed view is presented of the dynamics of the June–August Hadley Cell, as given by ERA data for the period 1981–2010, with an emphasis on the dynamics of the upper branch. The steady and transient northward fluxes of angular momentum have a very similar structure, both having a maximum on the Equator and a reversal in sign near 12°S, with the transient flux merging into that associated with eddies on the winter subtropical jet. In the northward absolute vorticity flux, the Coriolis torque is balanced by both the steady and transient fluxes. The overturning circulations that average to give the Hadley Cell are confined to specific longitudinal regions, as are the steady and transient momentum fluxes. In these regions, both intraseasonal and synoptic variations are important. The dominant contributor to the Hadley Cell is from the Indian Ocean and west Pacific regions, and the maxima in OLR variability and meridional wind in these regions have a characteristic structure associated with the Westward-moving Mixed Rossby–Gravity wave. Much of the upper tropospheric motion into the winter hemisphere occurs in filaments of air from the summer equatorial region. These filaments can reach the winter subtropical jet, leading to the strengthening of it and of the eddies on it, implying strong tropical–extratropical interaction.

KEYWORDS

angular momentum, filaments, Hadley Cell, OLR, tropical convection, tropical–extratropical, vorticity, WMRG

1 | INTRODUCTION

The Hadley Cell is one of the basic concepts in weather and climate, a superb history of the early ideas on it having been summarised by Lorenz (1967). A more recent review was given in, for example, Schneider (2006). The zonal mean overturning circulation in a latitude–height plane for boreal summer is shown in Figure 1. The picture is dominated by the rising motion in the belt of deep convection in the Northern (summer) Hemisphere (NH) between the Equator and 20°N and the descending motion in the Southern (winter) Hemisphere (SH) subtropics near 30°S, with motion towards the summer hemisphere near the surface and a return flow towards the winter hemisphere in the upper troposphere. This boreal summer Hadley Cell is complemented by an austral summer Hadley Cell and a transition between the two in the equinoctial seasons, giving an annual average picture with two Hadley Cells almost symmetric about the Equator (Dima and Wallace, 2003).

Following the studies of Schneider (1977), Held and Hou (1980) developed the seminal theory for the existence and nature of Hadley Cells. In this theory, the Hadley Cells must exist to give a reduction of the upper tropospheric winds implied by thermal wind balance with tropical temperature gradients to a magnitude that could be produced by angular momentum conservation in movement from the Equator. Angular momentum conservation in the upper branch of the Hadley Cells, together with frictional dominance near the surface, are basic to deductions from the theory. The annual average theory was extended to the four seasons by Lindzen and Hou (1988). Plumb and Hou (1992) gave a similar discussion in terms of a zero absolute vorticity limit for the zonal wind balancing an equilibrium tropical temperature gradient, beyond which Hadley Cell over-turnings must occur. Based on the large-scale vorticity equation, Emanuel (1995) suggested that the zero absolute vorticity limit should apply in a three-dimensional (3-D) Hadley Cell.

In the original Held and Hou theory, the extent of the Hadley Cells was determined through energetic consistency. However, Held (2000) discussed the alternative idea that deep baroclinic instability may provide the limit to their extent.

As recognised by Held and Hou, angular momentum conservation from zero velocity at the Equator moving to another latitude, φ, gives a zonal wind, $u = u_{\mathrm{AM}} = a\Omega\sin^2\varphi/\cos\varphi$, that is many times larger than that observed. This means that eddy angular momentum mixing processes must be of order-one importance, as proposed earlier by Jeffreys (1926). The importance of the momentum flux associated with higher-latitude eddies was stressed by Schneider (2006), and the emphasis has shifted to the key role played by midlatitude eddies and their momentum flux in many subsequent papers on Hadley Cells and their latitudinal extent.

As will be discussed in Section 3, for consideration of longitudinally limited regions, angular momentum has the problem that pressure gradient terms tend to dominate in changes following air parcels. Because of this, analyses based on vorticity and potential vorticity (PV) can be more illuminating and will mostly be used in this article.

For solstitial Hadley Cells, with air moving from one hemisphere to the other, it is helpful to consider the inertial motion that would take place in the absence of pressure forces. As calculated and discussed by Paldor and Killworth (1988), air that crosses the Equator will turn around and return to its original hemisphere. If the air is moving eastward crossing the Equator it will continue to move eastwards, undulating back and forward across the Equator. If it is moving westwards it can perform more of a figure-of-eight around the Equator. This is the result of linear theory. However, in the nonlinear case, the air conserves its vorticity (or PV). This leads to the air parcel that has crossed the Equator having the opposite sign in vorticity (or PV) compared with the ambient air, and there is the possibility of local inertial instability with the air accelerating away from the Equator.

Rodwell and Hoskins (1995) analysed the low-level flow that moves from the southern Indian Ocean, crosses the Equator beside the East African Highlands and carries moisture into the Indian Monsoon heating region. PV sources and sinks near the surface were found to be crucial for the assimilation of the air into the NH. If the PV sources are not strong enough, the air tends to move back towards the Equator and misses India. In addition, the air moving rapidly into the NH carries its negative PV with it and forms a strip of minimum PV. The strength of the Somali Jet is thought to be associated with the consequent inertial instability and acceleration down the pressure gradient. In Tomas and Webster (1997), inertial instability was seen as crucial to the location and strength of near-equatorial convection.

In the upper branch of the Hadley Cells, away from the region of ascent and deep convection in the region of the upward branch, the heating and friction should be small, so that PV is nearly conserved moving with the air. Air moving from the summer hemisphere should therefore carry its "wrong-signed" PV deep into the winter hemisphere. However, this would be expected to lead to instability. In addition, this broad occurrence of summer hemisphere PV deep in the winter hemisphere is not seen in analyses. These considerations raise the question of how air in the upper branch of the solstitial Hadley

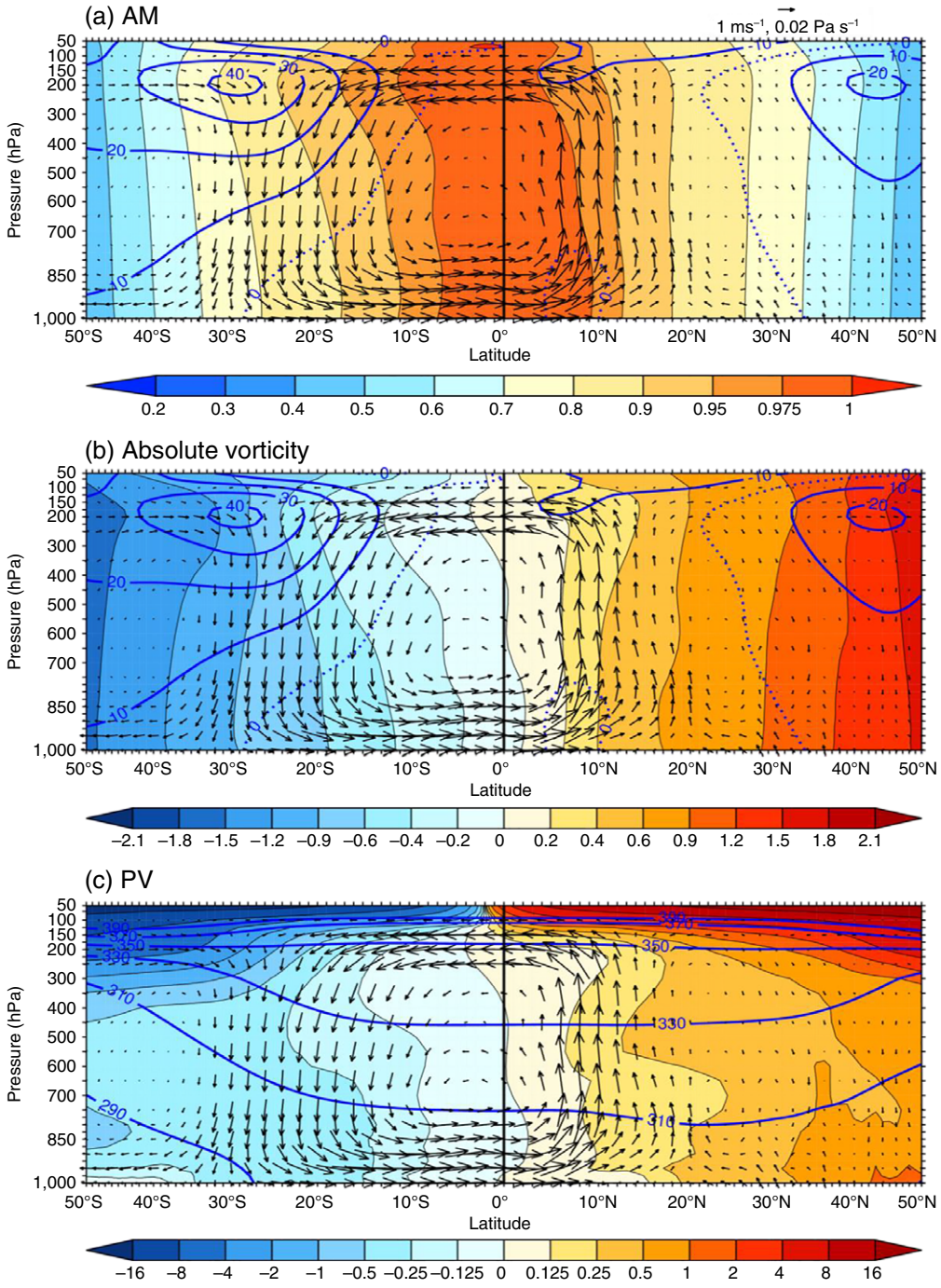

FIGURE 1 The 30-year mean JJA Hadley cell. In each panel the meridional circulation (V, ω) is shown by vectors, with the scale at the top right. In the top two panels U is shown by dark blue contours with interval 10 m·s^{-1}, and with the zero-contour dotted. In the lower panel the dark blue contours are for the isentropes, with interval 20 K. The abscissa is the sine of the latitude. The fields shown with block contours are: (a) angular momentum (unit $a^2\,\Omega$), (b) the vertical component of absolute vorticity (unit Ω) and (c) potential vorticity (PV) (unit PVU)

Cells can irreversibly cross the Equator and approach the subtropical jet.

The aim of this article is to investigate some of the questions raised using diagnosis of European Centre for Medium-range Weather Forecasts (ECMWF) re-analysis ERA-Interim data for boreal summer, June to August (hereafter JJA). The structure of the article is that in Section 2 the data and diagnostics used are briefly described. The zonally averaged view of the Hadley Cell in terms of angular momentum, vorticity and potential vorticity will be discussed in Section 3. The zonal and temporal variation of meridional flows in the Hadley Cell region are investigated in Sections 4 and 5, respectively. Events with strong convection and associated cross-equatorial flow are illustrated in Section 6. Section 7 contains a concluding discussion. A summary of some relevant equations is given in the Appendix.

2 | DATA AND DIAGNOSTICS

Data used in this study are ECMWF ERA-Interim re-analysis horizontal winds (u, v), vorticity, and

geopotential height (Z) for the 30-year period from 1981 to 2010. The fields are available 6-hourly with horizontal resolution of about 0.7° and at 37 pressure levels from 1,000 to 1 hPa. In addition, potential vorticity is available on a limited number of isentropic levels. Detailed information on the data can be found in Dee *et al.* (2011). NOAA interpolated daily outgoing long-wave radiation (OLR), which has a horizontal resolution of 2.5°×2.5° (Liebmann and Smith, 1996), is also used as a proxy for convection.

Three variables will form the basis for the analysis in this article. They are specific angular momentum, A, the vertical component of absolute vorticity (hereafter generally referred to as vorticity), ζ, and potential vorticity (PV), P, and they are defined in the Appendix in Equations A1–A3, respectively. Here the latitudinal coordinate used is $\mu = \sin\varphi$, where φ is the latitude, and the horizontal velocity variables are $U = u\cos\varphi$ and $V = v\cos\varphi$. The relationship between the latitudinal gradient of A and ζ is given in Equation A6. Taking a zonal average, denoted by [], gives (as in Equation A7):

$$\frac{1}{a}\frac{\partial[A]}{\partial\mu} = -a\,[\zeta]. \tag{1}$$

Thus, in a zonal average the latitudinal gradient of A is proportional to ζ. In particular, $[A]$ being uniform with latitude implies that $[\zeta]$ is identically zero.

On large horizontal scales the vertical component of the vorticity term dominates in PV (Equation A4). In low latitudes, the variation in vorticity dominates over variations in static stability, and so to a good approximation PV and ζ are related by a stratification that is a function of the vertical coordinate only (Equation A5). In higher latitudes the variation of the stratification can be of equal importance to that of ζ in the PV, and this approximation is not valid.

The equation for the material rate of change of A is given in Equation A8. As well as a frictional term, the equation for A contains a zonal pressure gradient term that in general means that arguments for material changes in A must take the pressure field as known. The pressure gradient force does not appear explicitly in the equations for ζ and PV. On a fluid parcel, ζ can change only through vortex stretching (and a twisting that is negligible on large scales) as well as a frictional torque, but PV only changes though frictional and diabatic processes.

The zonally averaged equation for A, when written in the flux form (Equation A9), shows that A changes due to the convergences of horizontal and vertical fluxes of A and to friction. However, it is more convenient here to use the zonally averaged equations for A (and U) and ζ in the forms given in Equation A10 and A11:

$$\frac{\partial[A]}{\partial t} = a\frac{\partial[U]}{\partial t} = -\frac{\partial}{\partial\mu}[UV] - a\frac{\partial}{\partial p}[\omega U] - af[V] + [F], \tag{2}$$

$$\frac{\partial[A]}{\partial t} = a\frac{\partial[U]}{\partial t} = a[V\zeta] - a\left[\omega\frac{\partial U}{\partial p}\right] + [F]. \tag{3}$$

Given that the terms involving ω are likely to be smaller, and in the long-term average the tendency terms will be very small for small frictional torque, Equation 2 emphasises the balance between meridional momentum flux convergence and the Coriolis force, and Equation 3 emphasises the role of meridional vorticity fluxes. These are also highlighted in the flux form of the zonally averaged vorticity equation (Equation A12):

$$\frac{\partial[\zeta]}{\partial t} = -\frac{1}{a}\frac{\partial}{\partial\mu}[V\zeta] + \frac{1}{a}\frac{\partial}{\partial\mu}\left[\omega\frac{\partial U}{\partial p}\right] - \frac{1}{a^2}\frac{\partial}{\partial\mu}[F]. \tag{4}$$

It should be noted that the absolute vorticity flux can be written as the sum of the Coriolis torque and the flux of relative vorticity, ξ:

$$[V\zeta] = f[V] + [V\xi]. \tag{5}$$

It will prove useful to make a decomposition of the meridional flux of both U and ξ based on a time average (below this will be for the JJA 30-year period), denoted by an over-bar, and deviations from it by a prime. Then:

$$[\overline{UV}] = [\overline{U}\,\overline{V}] + [\overline{U'V'}], \tag{6}$$

$$[\overline{V\zeta}] = f[\overline{V}] + [\overline{V}\,\overline{\xi}] + [\overline{V'\xi'}]. \tag{7}$$

[Correction added on 20 January 2020, after first online publication. Equations (6) and (7) have been corrected in this version.]

In each case, the term involving only products of time-averages will be referred to as the steady flux, and the final term will be referred to as the transient flux. It should also be noted that the momentum and vorticity fluxes are related:

$$[V\xi] = -\frac{1}{a}\frac{\partial}{\partial\mu}[UV] - \left[U\frac{\partial\omega}{\partial p}\right]. \tag{8}$$

This relationship gives the equivalence of the two forms of the equation for A and U given above (Equations 2 and 3).

In the absence of frictional and diabatic processes, the near material conservation of P and θ away from the convective regions means that P can trace the motion of upper tropospheric air on θ surfaces and will be used for that

in this article. The inversion properties of PV also mean that implications can be drawn from its distribution for the dynamic and thermodynamic state of the atmosphere (Hoskins *et al.*, 1985).

3 | ANGULAR MOMENTUM, VORTICITY AND PV CONSIDERATIONS

Figure 1a–c show the zonally averaged mean meridional circulation for JJA with colour block contours of A, ζ and PV, respectively. Also shown on each are contours of zonal mean U. The winter subtropical jet (STJ) is apparent, centred near 200 hPa and 30°S. The JJA Hadley Cell is clear in each, with its ascent near 10°N, descent near 20°S, northward motion mostly below 850 hPa and southward motion mostly between 150 and 250 hPa. Clearly, the northward-moving air in the lower branch of the Hadley Cell moves through contours of all three variables. In fact, with the frictional reduction in winds near the surface, the values of A and ζ there are close to those for zero winds, that is $a^2\Omega^2\cos^2\varphi$ and $f = 2\Omega\sin\varphi$, respectively. In the upper branch of the Hadley Cell, the contours of each variable are deformed as if partially advected by the southward-moving air. However, A is far from uniform, and consistent with this, ζ, which is proportional to its gradient (Equation 1) and PV, though reduced in magnitude at low latitudes (as is clear by comparing with the low-level contours), are certainly not zero. The fact that ζ is generally closer to f than zero over the Southern Hemisphere subtropics is consistent with the actual subtropical jet maximum being very much smaller than the value that would be associated with the conservation of A in the upper branch of the Hadley Cell.

Looking in more detail at the upper branch of the Hadley Cell in Figure 1a, from 10°N to the Equator the value of A increases in the direction of the southward motion. From 5°S to 25°S, the value of A decreases. In the context of the zonally averaged momentum equation, Equation 1, the fact that the vertical momentum flux convergence and any frictional term are expected to be relatively small means that in the time average the Coriolis force associated with the mean southward-moving air must be nearly balanced by the horizontal momentum flux convergence. Figure 2 shows latitude–pressure pictures of the steady and transient horizontal momentum fluxes (Equation 6). The large southward transient momentum flux centred near 30°S at 250 hPa is associated with transients on the SH winter STJ. Less discussed, though highlighted by Dima and Wallace (2003) is the shallow region of northward momentum flux centred near the Equator and 150 hPa. This is strongest in the steady flux, but also present with a very similar structure in the transient flux. The convergence of this flux from the Equator to about 10°N provides the required balance with the Coriolis force here (f positive and V negative). In the SH, the divergence of this equatorial momentum flux, together with that of the transient flux on the SH STJ, provide the required balance with the Coriolis force (f negative and V negative) from about 5 to 25°S. The important role in the momentum balance of the steady and transient momentum flux centred close to the Equator and in a shallow layer near 150 hPa is evident from this discussion.

The vorticity flux form of the zonally averaged momentum equation, Equation 3, also provides insight into the dynamics in the upper troposphere. As discussed in Section 2, except perhaps in the latitudes of deep convection and the ascending branch of the Hadley Cell, in the zonal average in the upper troposphere the Coriolis term must be nearly balanced by the meridional flux of relative vorticity to give a near-zero flux of absolute vorticity. The absolute vorticity flux (labelled "tot") and the decomposition of it as in Equation 7 (with the terms labelled "Cor", "steady" and "trans", respectively) are shown in Figure 3 for JJA 2009 and at the 200 hPa level. The latter is a compromise between 150 hPa, which is more suitable for the deep Tropics, and 250 hPa, which is more suited to higher latitudes. Consistent with expectation, there is generally a large compensation between the terms so that the total vorticity flux is indeed relatively small. Between the Equator and 10°N both the steady and transient fluxes act to compensate the Coriolis term, but here the cancellation is only partial, consistent with the possibility of a frictional term associated with the convection in this region. The ECMWF model used in their analysis system does contain a parametrization of cumulus momentum transport. In the latitudes 5°S–25°S the Coriolis term is balanced by the steady and transient vorticity fluxes. The former is about twice as large, but both are important. Further analysis shows that the contribution of the time-varying zonal mean Hadley Cell ($\overline{[V]'[\xi]'}$) to the transient flux is negligible, so that the zonally asymmetric eddy component ($[\overline{V'^*\xi'^*}]$) is totally dominant in the transient vorticity flux. It should be noted that the steady and transient vorticity fluxes for this 1 year are consistent with the latitudinal gradients at 200 hPa of the momentum fluxes shown in Figure 2 for the 30 years.

Both momentum and vorticity perspectives show that in the upper troposphere, tropical zonally asymmetric steady and transient motions play crucial and similar roles in the dynamics of the Hadley Cell. Following this insight, the nature of the steady zonal asymmetries and the transient motions will be investigated in the next two sections.

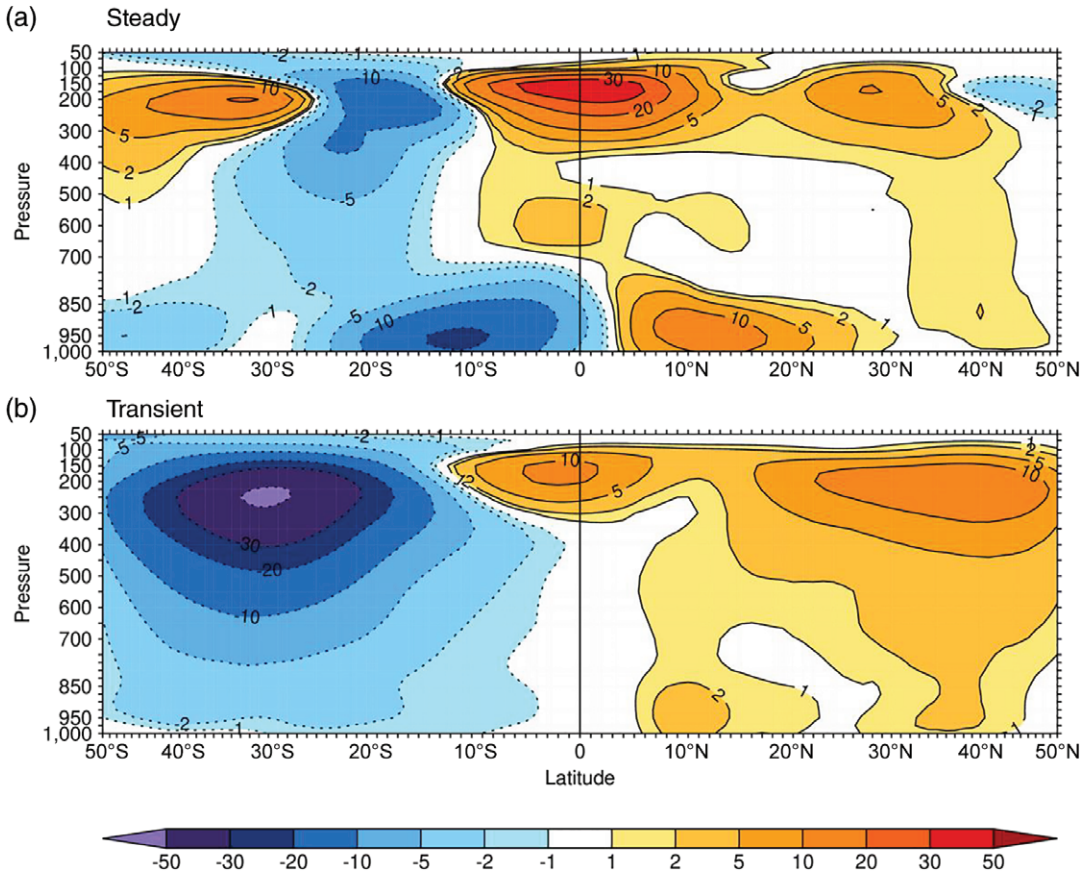

FIGURE 2 Northward fluxes of angular momentum by (a) the steady and (b) the transient motions, as defined in Equation 6. The contour interval is not uniform. Contours at negative values are dashed. The unit is $m^2 \cdot s^{-2}$ [Correction added on 13 January 2020, after first online publication. Figure 2 has been corrected in this version.]

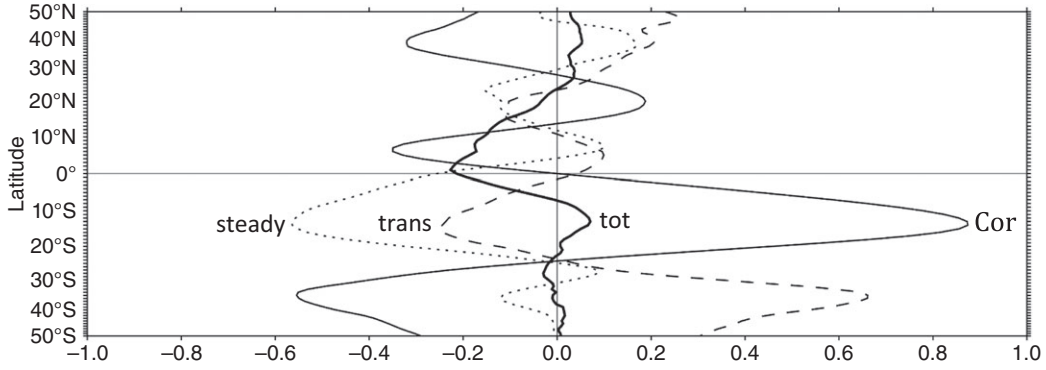

FIGURE 3 The northward flux of absolute vorticity at 200 hPa for JJA 2009, and its component split as in Equation 7. The total flux is denoted "tot". The Coriolis torque, the steady flux of relative vorticity and the transient flux are denoted "Cor", "steady" and "trans", respectively. The unit is 1×10^{-4} m·s^{-2}

4 | THE 3-D STRUCTURE OF THE TIME-MEAN HORIZONTAL MOTION ASSOCIATED WITH THE HADLEY CELL

First the structure of the time-mean Hadley Cell meridional motion is illustrated in two ways. The latitude–longitude structure of the time-mean motion in the upper and lower troposphere and of the OLR is given in Figure 4a,b and the longitude–height section of V averaged from 10°S–5°N in Figure 5.

The mean winds in the lower troposphere (arrows on Figure 4b) exhibit the northward flows from the SH and across the Equator that average to give the 950 hPa

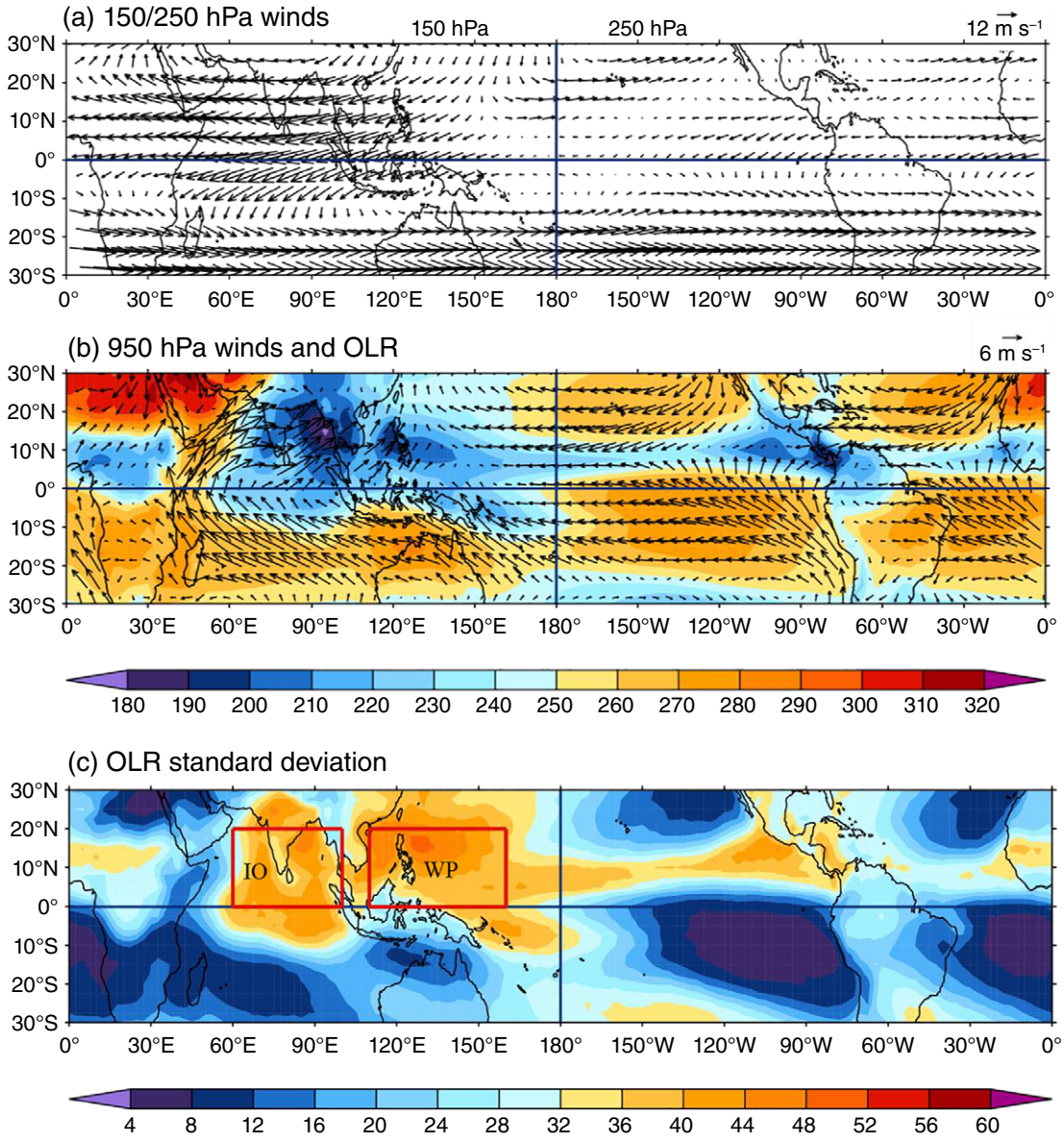

FIGURE 4 Thirty-year time-mean horizontal winds and OLR statistics. (a) Upper tropospheric vector winds, at 150 hPa in the Eastern Hemisphere and 250 hPa in the Western Hemisphere; unit at top right. (b) Lower troposphere, 950 hPa, vector winds and time-mean OLR ($W \cdot m^{-2}$). (c) Time-mean of the seasonal standard deviation of OLR. The boxes shown in the lower panel are the IO and WP regions defined in the text

component of the lower branch of the Hadley Cell. The dominant cross-equatorial motion is associated with the flow from the southern Indian Ocean into the South Asian and the west Pacific regions of convection. Also clear are the flows from the SH into the east Pacific and Atlantic intertropical convergence zone (ITCZ) heating regions. Each of these Trade Wind flows changes from southeast to southwest as it crosses the Equator. In the upper troposphere (Figure 4a) there is a strong return flow in the Indian Ocean/west Pacific sector and weaker return flows in the ITCZ regions. It should be noted that in Figure 4 the upper troposphere is shown at 150 hPa in the Eastern Hemisphere and 250 hPa in the Western Hemisphere, and the lower troposphere at 950 hPa. These levels are chosen to capture the maxima in most regions. However, they are not optimum for the African sector where, as will now be seen, 200 and 750 hPa would be more suitable.

In Figure 5 a 15° band of latitudes from 10°S to 5°N is used for averaging the meridional wind, this being sufficiently narrow to delineate the structure of the cross-equatorial motion and broad enough to indicate the general structure of the entire upper and lower branches of the Hadley Cell. The topography close to the Equator is indicated below the panel. Consistent with Figure 4, the

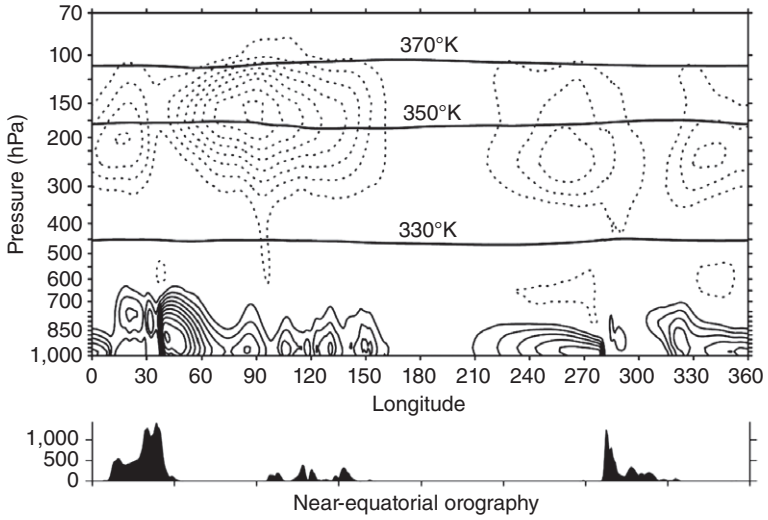

FIGURE 5 Thirty-year time-mean v averaged between 10°S and 5°N. The contour interval is 1 m·s^{-1}, with the zero contour omitted and negative contours dashed. Also shown are the isentropic levels 330, 350 and 370 K. At the bottom of the figure is near-equatorial orography, and the scale on the left is in m

Hadley Cell is seen to be made of both upper and lower branches in the Indian Ocean/west Pacific, the east Pacific, the Atlantic and Africa. At low levels in the first region, it is apparent that the strong cross-equatorial motion near the Eastern Highlands of Africa is accompanied to the east by other maxima that are generally also hugging the eastern sides of islands. As in Rodwell and Hoskins (1995), it appears that the extra friction they provide may be important in enabling the air to cross the Equator. However, the recent experiments of Zhuang and Duan (2019) suggest that the islands act to separate the cross-equatorial flow and even slightly reduce its total mass transport. In the east Pacific and Atlantic, the shallow southerly flows deepen slightly to the west. Over Africa, as will be seen in Figure 5 below, the motion towards the summer hemisphere occurs over the high plateau and is therefore not seen in Figure 4b.

The return flow in the various regions in the upper troposphere shows less detailed structure. Except over Africa, the return flow in the Eastern Hemisphere maximises near 150 hPa. However, in the Western Hemisphere, in the east Pacific and Atlantic, the maximum return flow is closer to 250 hPa, consistent with the convection there being generally not as deep. Also over the Atlantic, and to a lesser extent the east Pacific, there is a weak return flow between 500 and 700 hPa, which leaves its signature on the zonally averaged Hadley Cell motion (Figure 1). This is consistent with there being some shallow convection in these ITCZ regions. For later reference, it should be noted that the 370 K θ-level is in the upper part of the Indian Ocean/west Pacific region of southerly flow, and the 350 K θ-level is in the lower part here and in the upper part in the east Pacific and Atlantic.

The mean OLR is shown in colour in Figure 4b. The dominant region of implied strong convection is that centred on South Asia and the Philippines. The low-level flow in this region is the major contributor to the lower branch of the zonally averaged Hadley Cell, and feeds into it moisture from the southern Indian and west Pacific Oceans. Also clear are the east Pacific and Atlantic ITCZs with their inflow from the south, and the continent of Africa, for which the inflow is at a higher level.

We now turn to the horizontal structure of the upper tropospheric momentum fluxes, whose role in the angular momentum budget were discussed in Section 2 and for which zonal average sections were shown in Figure 2. In Figure 6 are presented longitude–latitude pictures of the steady and transient momentum fluxes for the upper troposphere (150 and 250 hPa in the Eastern and Western Hemisphere, respectively). It is striking that the signature of positive momentum fluxes centred near the Equator and negative fluxes poleward of about 10°S–15°S is seen to occur in each of the Indian Ocean–west Pacific, east Pacific, Atlantic and African sectors in both steady and transient momentum fluxes. The positive signature is larger in the steady flux, and the negative flux in the STJ latitudes is dominated by the transient flux. In the Indian Ocean–Australian sector, the latter is more evident at 250 hPa, which is closer to tropopause level there.

5 | THE TEMPORAL BEHAVIOUR ASSOCIATED WITH THE HADLEY CELL

When compared with the mean OLR (Figure 4b), the standard deviation of OLR (Figure 4c) shows maximum values in similar tropical regions. Its magnitude is comparable with the variation of the mean OLR from convective to non-convective regions, indicating that the variability is sufficiently large that the convection tends to vary between being large and being almost absent. The dominant signal

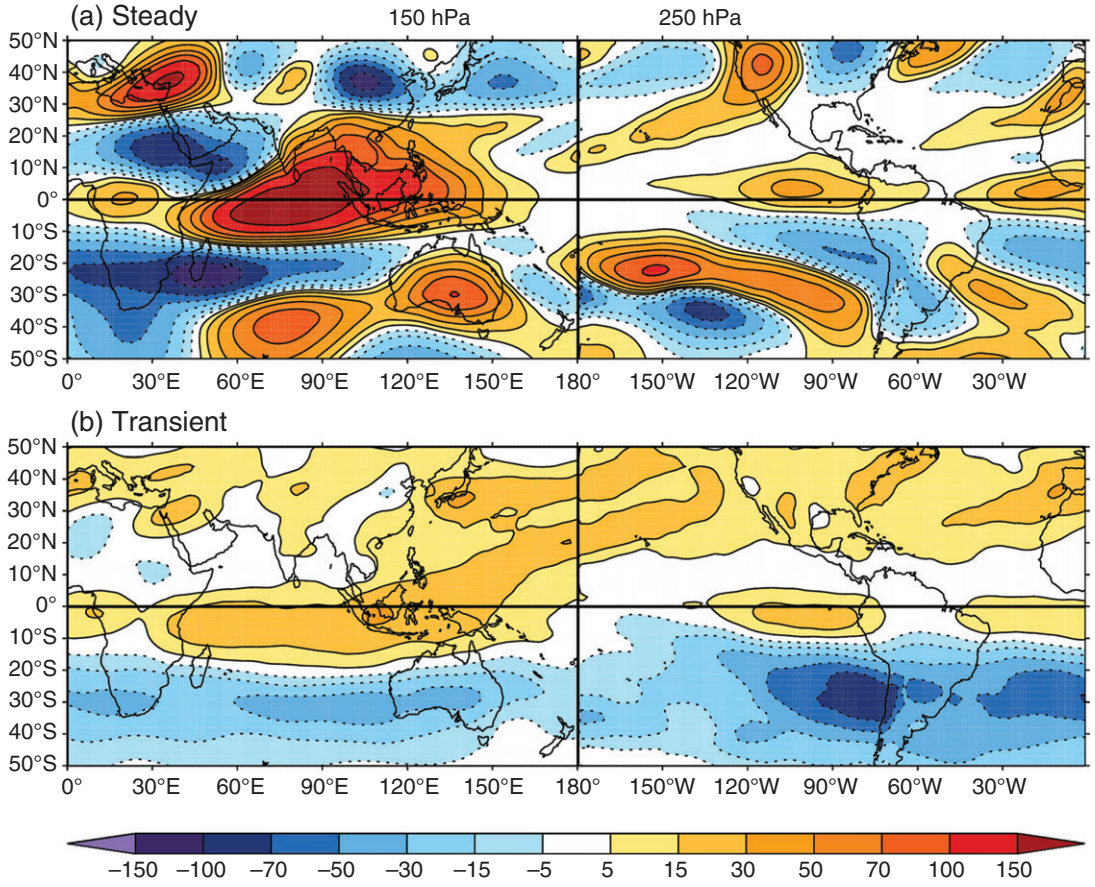

FIGURE 6 Thirty-year time-mean northward flux of angular momentum in the upper troposphere, at 150 hPa in the Eastern Hemisphere and 250 hPa in the Western Hemisphere. (a) Steady, and (b) transient. The unit is $m^2 \cdot s^{-2}$

is again the south Indian and Philippine regions, but this time there is an indication of a break between the two. Consequently, in some of the analysis below, the OLR in the boxes shown will be considered separately and they will be referred to as the Indian Ocean or IO Region (60–100°E, 0-20°N) and the Warm Pool or WP Region (110–160°E, 0–20°N).

To illustrate the nature of the transient behaviour, Hovmöllers of 5°N–10°S v at 150 and 950 hPa, and 0–20°N OLR for one JJA season are presented in Figure 7. An El Niño neutral year, 2009, is used for this illustration. The average OLR for this season is very similar to that shown for the 30-year average in Figure 4a. The Hovmöller for OLR (Figure 7c) shows low (blue colours), indicating cold cloud tops and deep convection for much of the time in the Indian Ocean/west Pacific, some of the time in the east Pacific sector (240°E–280°E) and occasionally in the Atlantic/West African sector (340°E–30°E). However, the transient nature of the OLR minima is also clear in each region. In the Indian Ocean there are weeks with more convection and some with less. In all the sectors, there are clear indications of westward-moving extrema with synoptic space- and time-scales. Separate OLR Hovmöllers for the latitudes 0°–10°N and 10°–20°N show that the westward-moving synoptic signature is mostly derived from the off-equatorial band. The meridional wind at 950 hPa, Figure 7b, shows that the southerlies seen in Figure 5 that make up the lower branch of the Hadley Cell also have significant transient behaviour on synoptic space- and time-scales. Again, these transients mostly tend to move westwards. When contours of 950/150 hPa wind and OLR are superimposed on each other (not shown) considerable evidence of coherence between the two fields is found over time-scales of a few days.

At 150 hPa (Figure 7a) the westward movement of both maxima and minima in the meridional flow are again apparent. In the Indian Ocean–west Pacific this is seen as an enhancement or diminishing of the southerly wind. A quite regular westward-moving transient behaviour on quite short space- and time-scales is apparent in the Atlantic–West Africa sector and east Pacific sectors, with some features moving westward from east of the zero meridian to the date-line. At 250 hPa in the Western Hemisphere (not shown), the southerly wind is more dominant

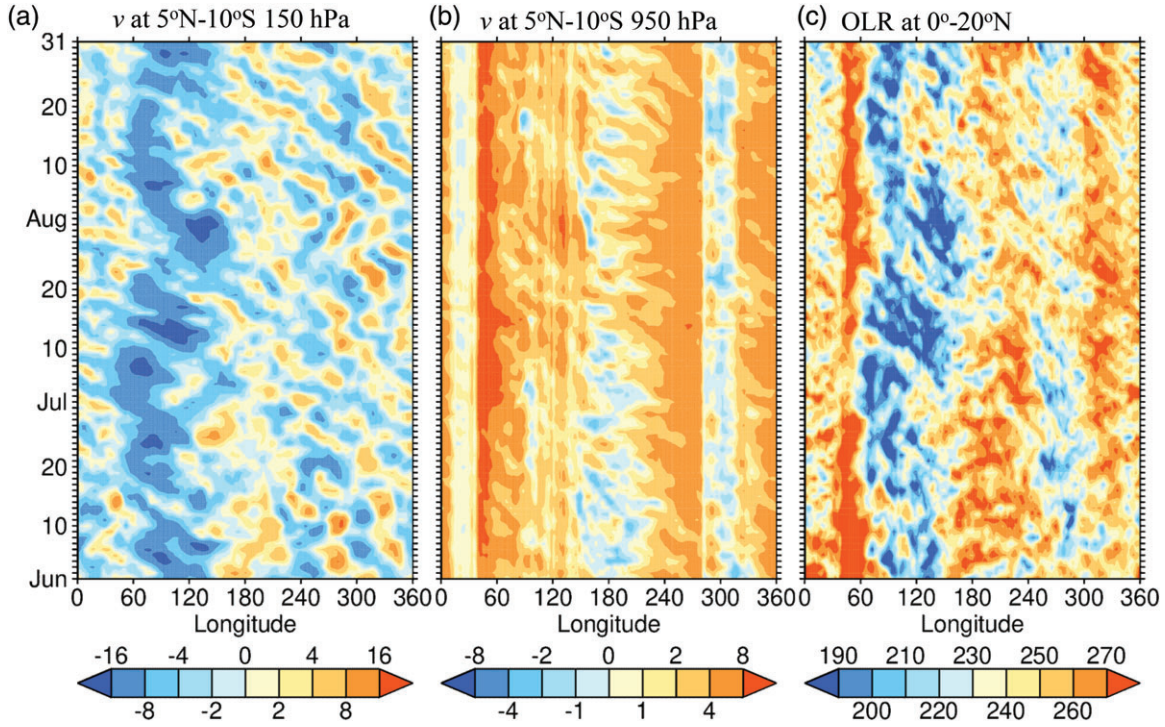

FIGURE 7 Hovmöllers for JJA 2009. (a) v at 150 hPa, averaged between 10°S and 5°N; (b) v at 950 hPa, averaged between 10°S and 5°N; (c) OLR averaged between 0° and 20°N. The unit is m s^{-1} for v and W m^{-2} for OLR.

than at 150 hPa and the dominance of westward movement is less apparent.

The synoptic time-scale transient behaviour found here is consistent with that found for the Eastern Hemisphere in JJA 1992 by Yang *et al.* (2007a; 2007b; 2007c). Using westward-moving OLR averaged from 4°N to 16°N, convectively coupled wave structures were found (Yang *et al.*, 2007b, Fig. 2) to have coherent behaviour in the upper and lower troposphere for more than a week, and also zonal wavelength of 45–50° and period 7–8 days.

Based on the 30-year period, power spectra for OLR at 0–20°N and for v averaged at 10°S–5°N and at 150/250 hPa are given in Figure 8. In both fields the importance of variability on both intraseasonal and synoptic (principally 4–9 days) time-scales is apparent. This is the case in the Indian Ocean–west Pacific region and in the ITCZ regions of the east Pacific and Atlantic. There are noticeable peaks near 9 days in the WP region and near 2 weeks in the IO Region. Further analysis (not shown) gives that these peaks come predominantly from the 10°N–20°N band.

To conclude this section, we consider the correlation behaviour of OLR in the IO and WP Regions. The autocorrelations are shown in Figure 9a. In the IO Region, there is a drop-off on synoptic time-scales, but then zeros about ±12 days and negative peaks near +15 and −17 days, and positive peaks again around +30 and −37 days, consistent with a 30–40-day period Intraseasonal Oscillation. For the WP Region these features are less apparent, though the autocorrelations reach near zero by about −20 and +17 days and are positive again near −40 days.

The correlation between OLR in IO and WP Regions (Figure 9b) shows positive values at +8 days, implying that the OLR in the WP Region has a negative extremum (maximum convection) about 8 days after the IO Region has one. The maximum near −30 days implies that IO Region has a negative extremum some 30 days after one in the WP Region. Taken together and assuming oscillatory behaviour, these are consistent with a period of 38 (8 + 30) days. Also, the WP Region has a negative peak 15 days before the IO Region has a positive peak. Together with 8-day lag referred to above, this is consistent with a half period for the IO Region of 23 (8 + 15) days and a full period of 46 days. Following Wang and Rui (1990) there have been many studies of the boreal summer IntraSeasonal Oscillation (ISO). The evidence here is for the eastward moving of the ISO in OLR with an approximate 40-day period and with the IO Region leading the WP Region by about 8 days.

The IO and WP Regions used here are similar to those of Lee and Wang (2016, hereafter LW) for their analysis of the regional boreal summer ISO, with the principal difference being that the latitudinal domain of LW extended

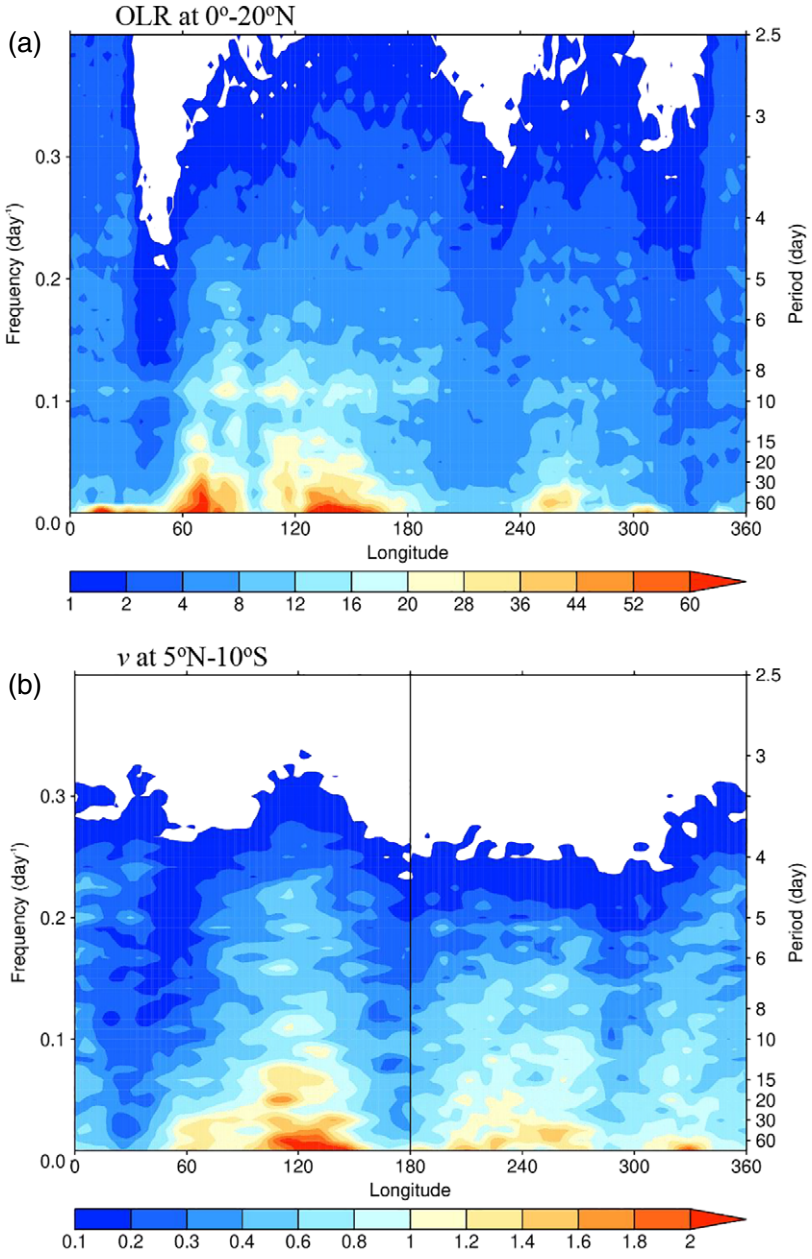

FIGURE 8 Power spectra for 30 years of (a) OLR averaged between 0° and 20°N, and (b) v at 150 hPa in the Eastern Hemisphere and 250 hPa in the Western Hemisphere, averaged between 10°S and 5°N. The power unit is $m^2\ s^{-2}$ for v and $W^2\ m^{-4}$ for OLR.

a further 10° on both the northern and southern sides. Comparing with the first two empirical orthogonal functions (EOFs) of their multivariate analysis of OLR and 850 hPa u in the two regions, it will be seen below that the OLR for their EOF2 in their IO Region and EOF1 in their WP Region correspond, respectively, to the OLR behaviour obtained here in the IO and WP Regions. In contrast to the eastward movement found here, LW showed a lack of such movement, but this was for their first EOFs in the two regions. Further analysis (not shown) gives that the major contribution to ISO time-scales found here comes from the 0–10°N band. Also, consistent with the analysis given above, LW found slightly longer ISO time-scales in the WP Region compared with the IO Region.

6 | EVENT BEHAVIOUR

In this Section, the major aim is to produce a more synoptic picture of the events that involve large negative OLR in the IO and WP regions, centred on South Asia and the Philippines, respectively. This will be done using data for the 30-year period, 1981–2010, and for 1 year, 2009.

As a context for this, we first show in Figure 10 PV on the 370 K isentropes averaged over 2009 JJA and for one typical analysis time, 1200 UTC on 1 August 2009. In the climatology (Figure 10a), the smooth picture shows the Asian Monsoon anticyclone (low PV) almost surrounded by higher values, as was discussed in Hoskins (1991). In particular, to the east high PV is advected southwards and then westwards in a broad tongue north of the Equator.

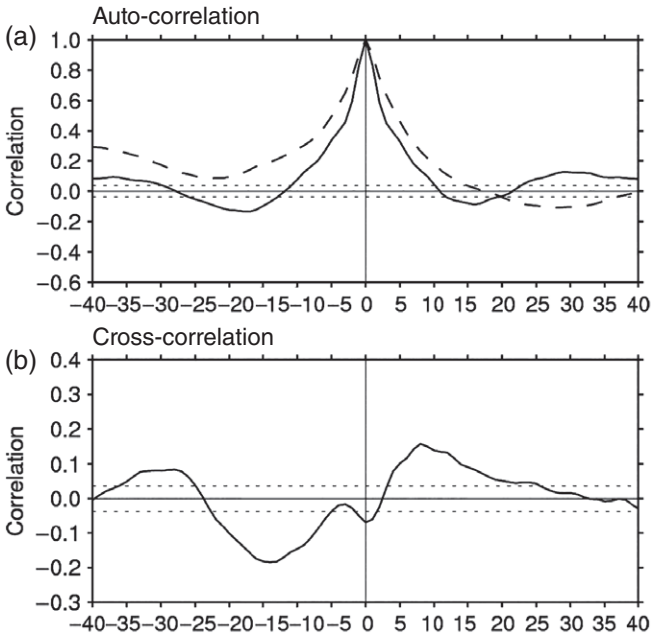

FIGURE 9 Auto- and cross-correlations of OLR in the IO and W Pregions based on 30-year data. (a) Autocorrelations of OLR in the IO region (solid line) and WP region (dashed line). (b) Cross-correlation of OLR in the IO and WP regions. Two horizontal dotted lines indicate correlation range exceed the 95% significance level

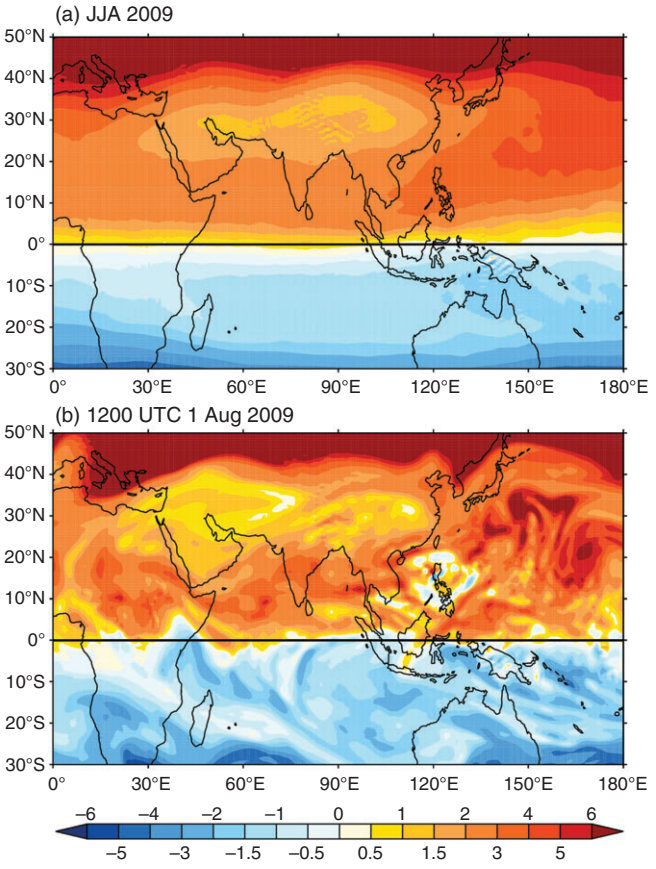

FIGURE 10 PV on the 370 K isentrope. (a) JJA 2009 time-mean; (b) 1200 UTC on 1 August 2009. The unit is PVU

At one analysis time, detailed structure associated with synoptic variability is striking, being even more so in movie loops over weekly periods (Video S1, Supporting information). Of interest here is the evidence of several filaments with near-equatorial PV values curved anticyclonically (anti-clockwise) into the SH. The videos show that such filaments can return to the tropical region, be mixed in the SH subtropics or reach the anticyclonic side of the STJ, like that near 90°E in Figure 10b. It is also seen in Figure 10b that over Africa (around 40°E), in a wave-like structure, negative PV from the SH has penetrated into the NH, reaching 10°N. This is consistent with Yang *et al.* (2018) who indicated that African Easterly Wave activity can be influenced by non-stationary Rossby waves propagating from the SH into NH in the upper tropospheric easterlies in that region. In the Philippines region some negative PV can be seen. Looking at the previous days, it is evident that these negative values appear in this region and are not advected from elsewhere. If these are real, they could be due to mesoscale generation associated with strong diabatic heating in a sheared environment.

Returning to the focus of this Section, Figure 11a,c show, for the 30-year period, fields regressed on IO Region OLR with zero lag. The OLR itself is given in Figure 11c. The low values in the whole IO Region area are indicative of the strong deep convection there, and the lack of extension into WP Region indicates the simultaneous absence of convection there. The lower tropospheric (950 hPa, Figure 11c) winds regressed on IO Region OLR show a strong flow starting from 35°S, around an enhanced Mascarene High and through a strong Somali Jet into the South Asian region of enhanced OLR. In the upper troposphere (150 hPa, Figure 11a), the return flow starts on the eastern side of the Asian Monsoon anticyclone and then involves a strong northeasterly flow from 10°N to 15°S in the western and central Indian Ocean. The flow then turns to a northwesterly direction and joins the anticyclonic side of the STJ. This is clearly consistent with the strong northward steady and transient momentum fluxes centred on the Equator and the southward fluxes south of 15°S discussed above and seen in Figures 2 and 6. The coloured field in Figure 11a shows the relative vorticity. Consistent with its near-equatorial origin, the air in the region in which the northwesterly flow approaches the STJ exhibits large anticyclonic relative vorticity.

All the same features are evident, and are even more striking, when the correlations are performed for JJA for the 1 year, 2009 (Figure 11b,d). In this 1 year, there are waves on the STJ and the upper tropospheric northwesterly from 15°S comes in slightly ahead of a trough.

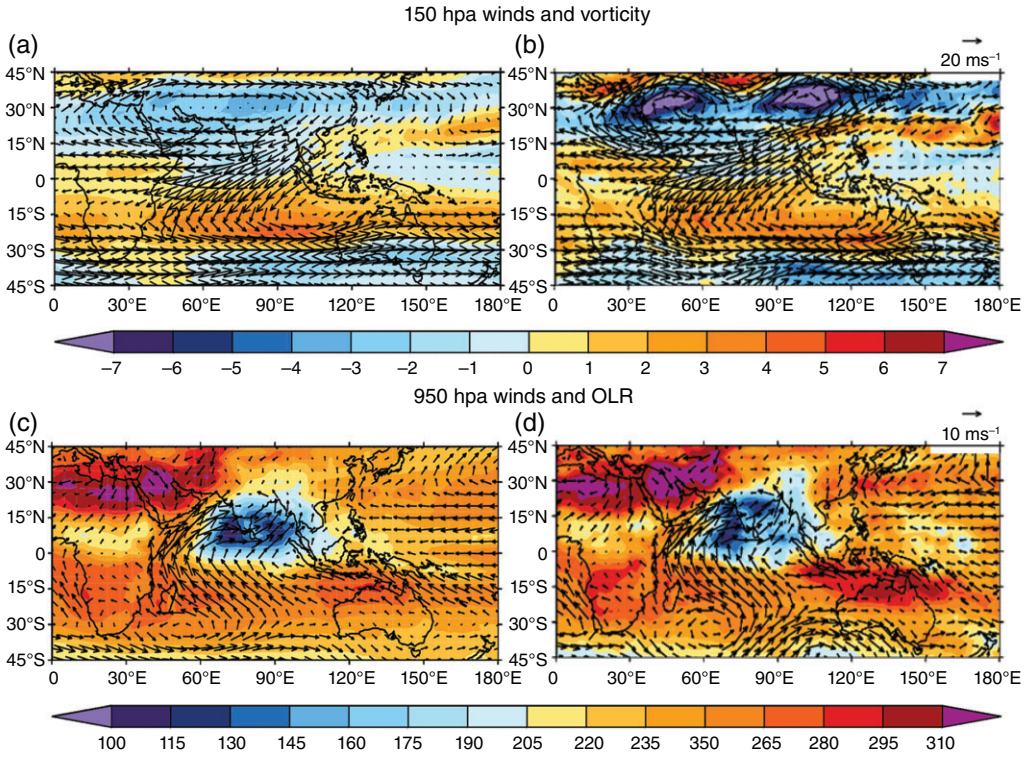

FIGURE 11 Fields regressed on OLR in the IO region for JJA for the 30-year climate (left; a,c) and for 2009 (right; b,d). The fields are 150 hPa wind vectors and relative vorticity block contours (top; a,b), and 950 hPa wind vectors and OLR block contours (bottom: c,d). The scales for the wind vectors are shown at the top right of the top and bottom rows. The OLR unit is W m^{-2}

Similar pictures for fields regressed on WP Region OLR are given in Figure 12. Referring first to the climate panels (left), in Figure 12 the OLR minimum is now mainly in the wider Philippines, WP Region. There is inflow to this around a broad anticyclonic region at 950 hPa. In the upper troposphere (Figure 12a), the return flow has a similar structure to that in Figure 11a but shifted some 40° to the east. For the single year, 2009, Figure 12d shows evidence of strong convection in the extended Philippines region and the inflow to it is around a very strong Australian high, which is well separated from the Mascarene high. The return flow in the upper troposphere (Figure 12b) is like that in the climate fields (Figure 12a) but the anticyclonic vorticity associated with it is more marked. There is a clear interaction with waves on the STJ, with the flow from the Tropics again joining ahead of a trough.

The time development of the upper tropospheric fields in these events in 2009 is illustrated in Figure 13 through fields regressed on OLR in the IO Region (left panels) and the WP Region (right panels) with lags of −3 days (top row) and +3 days (bottom row). In both cases, the return flow is largely limited to the near-equatorial region 3 days before the OLR minimum. Three days after the OLR minimum it is strongly interacting with the STJ and the waves on it. Associated with it, there is large anticyclonic vorticity.

The upper tropospheric behaviour in two events in 2009 is illustrated in Figure 14 with 370 K PV and 150 hPa winds for 8 July and 13 July. The general character of the two events is very similar to those given above in Figure 11 for the IO Region and in Figure 12 for the WP Region. The tongues of NH PV moving into the SH in the regions of strong cross-equatorial winds are consistent with the expected approximate material conservation of PV away from the convective region in the northern Tropics. Low magnitudes in PV are seen reaching to the STJs ahead of the troughs. The fact that the PV values here are not even closer to tropical NH values than they are may be because of some mixing in the atmosphere or because the ERA system itself introduces mixing.

The importance of both synoptic and longer time-scale variability in the OLR minima in the climatology for the WP Region is evident from Figure 15. Here, for lags −3 days, 0 and + 3 days with the OLR minima in the WP Region, are shown regressed OLR anomalies from the 30-year mean, near-equatorial 150 hPa full (raw) v and various components of it. The negative OLR anomaly grows and decays in the WP Region in the 6-day period. It is basically stationary but there is a hint of a small, more synoptic-scale component with some westward movement from day −3 to day 0. Full v is negative throughout the whole IO Region and WP region domain and throughout

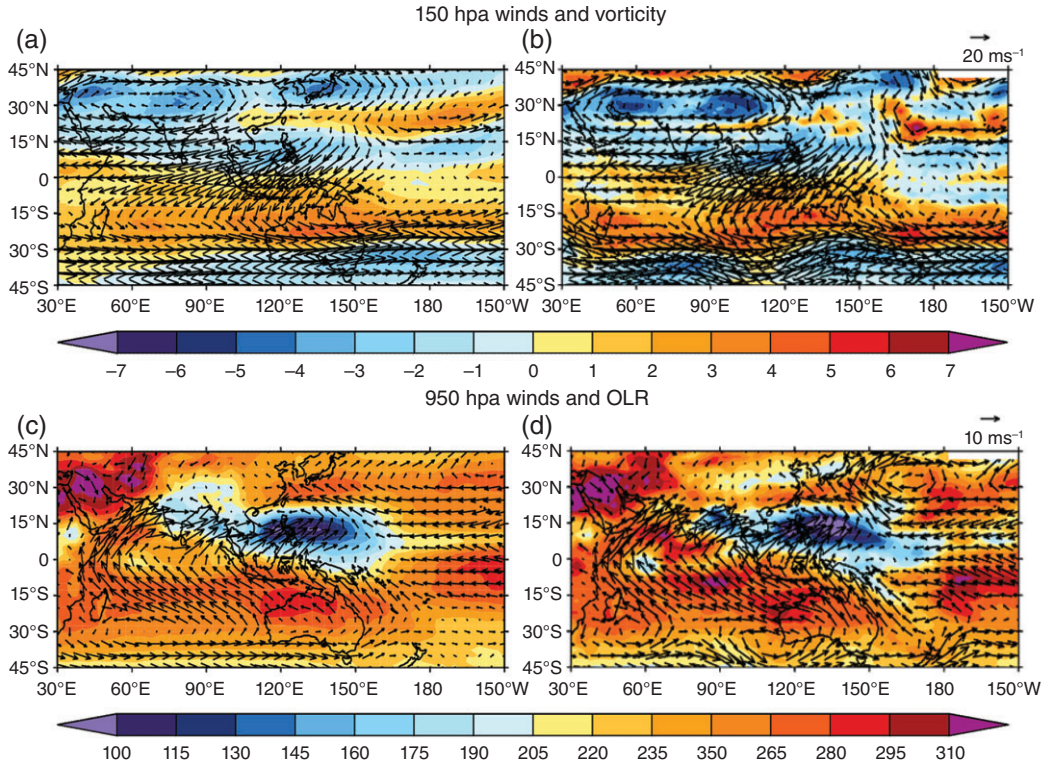

FIGURE 12 As in Figure 11 but for fields regressed on OLR in the WP region

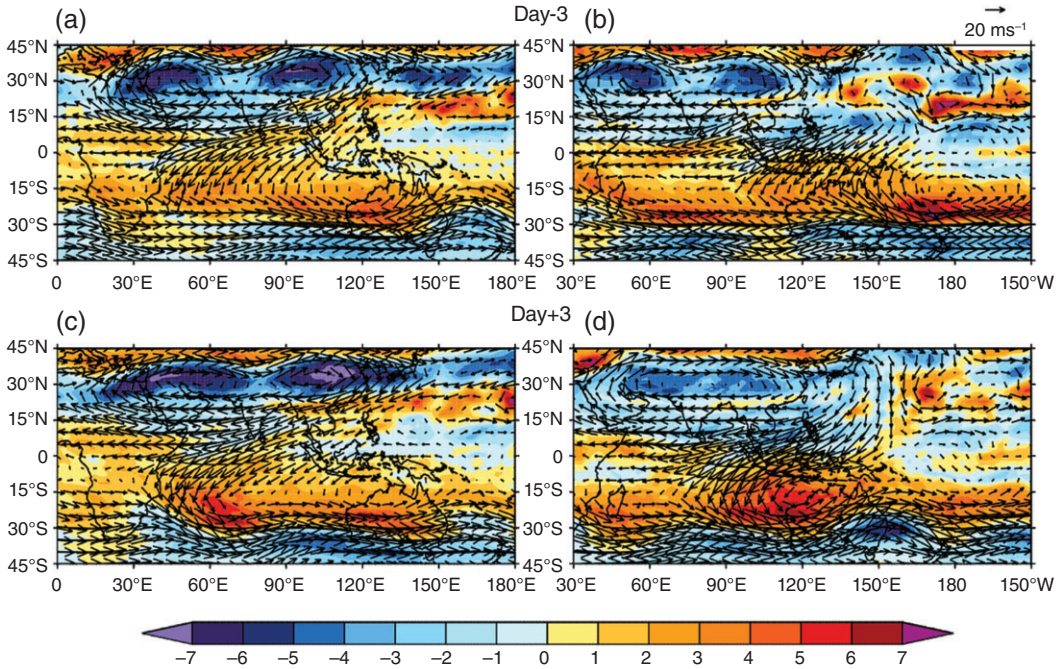

FIGURE 13 150 hPa winds and vorticity regressed on OLR in the IO region (left; a,c) and the WP region (right; b,d) for lag −3 days (top; a,b) and lag +3 (bottom; c,d) in JJA 2009

the period. The anomaly (departure from the 30-year JJA mean) in v grows to become about 70% of the full v in the WP Region at day 0 and decays with some westward movement on synoptic scales.

As mentioned above, Yang *et al.* (2007a; 2007b; 2007c) have shown that projection onto the horizontal structures of classic equatorial waves indicated that much of the real world near-equatorial synoptic behaviour in one summer

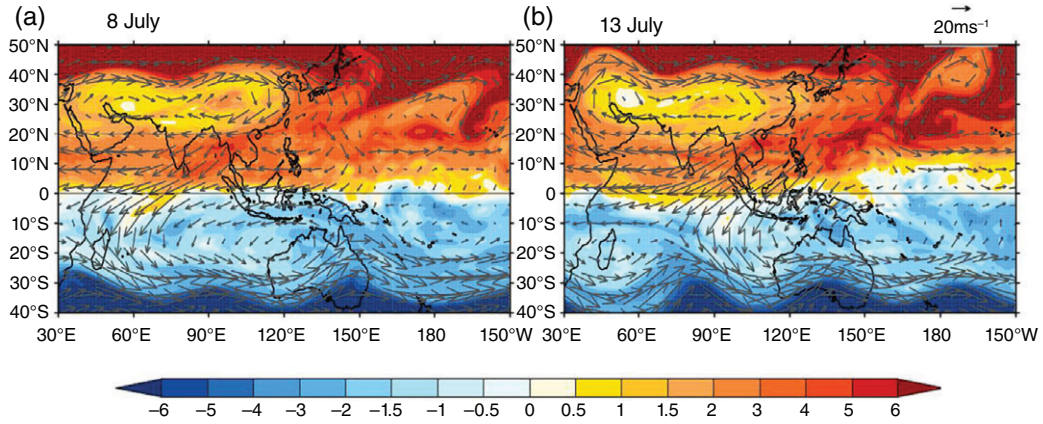

FIGURE 14 370 K PV and 150 hPa vector winds for (a) 8 July 2009 and (b) 13 July 2009

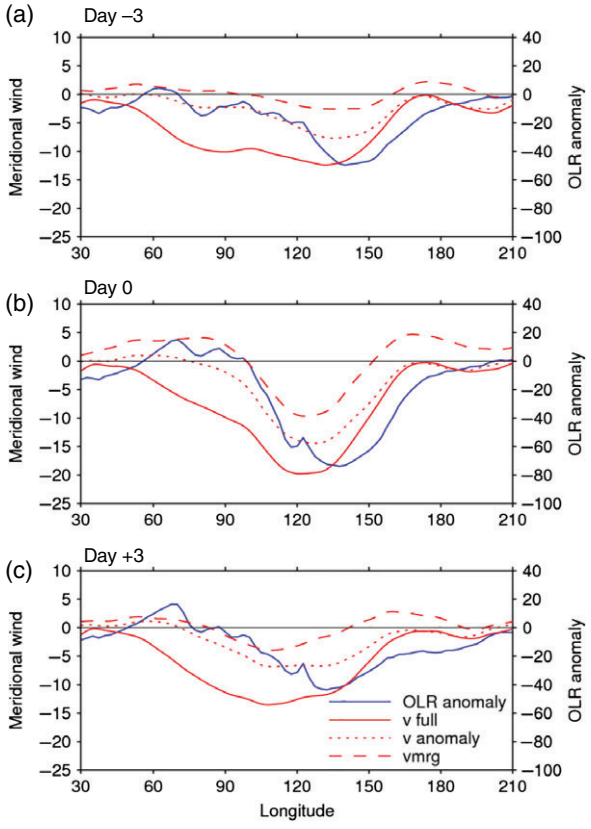

FIGURE 15 Fields at (a) day −3, (b) day 0 and (c) day +3 of OLR (0–20°N) and near-equatorial v (5°N–5°S) for the 30-year data for regressions on OLR in the WP region. Shown are the OLR anomaly (blue), 150 hPa v (continuous red line), and its anomaly (dotted red line). Also shown is the component of 150 hPa equatorial v associated with the projection onto the $n = 0$ equatorial MRG wave structures at 150 hPa (dashed red line). See text for more details

can usefully be related to these wave modes, even though many assumptions of the idealised theory are not strictly valid. The projections of the 150 hPa v-field (filtered to wave-numbers 2–40) onto the horizontal, $n = 0$ equatorial mixed Rossby–gravity wave structure is also given in Figure 15. The growth and decay, and westward movement are even more apparent for this component. At day 0 it comprises about 65% of the anomalous near-equatorial v. Yang *et al.* (2007a; 2007b; 2007c) showed the prominence of the $n = 0$ Westward-moving Mixed Rossby–Gravity (WMRG) wave in the Eastern Hemisphere in JJA 1992 and exhibited in Fig. 5 of Yang *et al.* (2007c) the horizontal structure typically associated with OLR minima in the Eastern Hemisphere. This looked very much like the 150 hPa structures shown in Figures 11–14 for the IO and WP Regions. It should be noted that for the Yang *et al.* (2007a; 2007b; 2007c) picture the data had been filtered to include only westward-moving anomalies with time-scales between 2 and 30 days. Here the MRG structure and the westward-moving behaviour seen in Figure 15 has been obtained with no such temporal filter.

7 | DISCUSSION

The aim of this article has been to investigate the dynamics of the Hadley Cell using data for the JJA season. Boundary-layer friction largely balances the Coriolis torque in the lower branch of the winter hemisphere Hadley Cell and the focus here has been on the upper branch where in general frictional processes can be expected to be minimal. Vertical advection of angular momentum is also expected to be very small in this layer. The implication is that in the time and zonal average, the meridional absolute vorticity flux, $[\overline{V\zeta}]$, must be zero to the first order. The splitting of this term into three different components has shown that the Coriolis torque is indeed nearly balanced by steady and transient relative vorticity fluxes. The former is larger, but both are important. From the momentum flux perspective, it has been seen that the tropical structures of the steady and transient fluxes are very similar, both having a northward maximum on the Equator, and reversal of sign in the belt 10–15°S. The

region of the southward transient momentum flux joins continuously with the large flux associated with eddies on the winter STJ.

The subsequent analysis of the longitude, latitude and time structures of the motions that average to give the Hadley Cell further add to the understanding that the Hadley Cell motions are the result of tropical convection and meridional circulations on longitudinally confined sectors and the enhancement of this convection during certain periods.

We now consider again the dynamical requirement that $[\overline{V\zeta}] \approx 0$. In the classic angular momentum conserving view, this is satisfied by $\zeta = 0$ everywhere in the upper branch of the Hadley Cell. Based on the diagnostics produced here, a better idealised model may be to separate into times/longitudes in which convection is strong and times/longitudes in which it is not. The former can be associated with near-equatorial PV and absolute vorticity being transported into the winter hemisphere, and the latter with more ambient conditions. Therefore, we assume:

where/when convection is active, $\zeta = 0$, and V is large, amplitude V_0, say;
elsewhere ζ is an ambient value, taken to be f, and $V = 0$.

If the convection occurs in a fraction of the longitudes, α_λ, and a fraction, α_t, of the time, then the wind and absolute vorticity in the upper branch of the Hadley Cell would be approximately αV_0 and $f\ (1-\alpha)$, respectively, where $\alpha = \alpha_\lambda \alpha_t$. The magnitude of the subtropical jet would then be αu_{AM}. Compared with $u_{AM} \sim 134\,\mathrm{m\cdot s^{-1}}$, the observed value, $\sim 42\,\mathrm{m\cdot s^{-1}}$ would be consistent with an active local Hadley Cell occurring about $\alpha = \alpha_\lambda \alpha_t = 0.3$ of the longitude–time. This contrasts with the more usual argument in terms of an axisymmetric Hadley Cell with stresses from extratropical eddies being responsible for reducing the zonal winds far below those given by angular momentum conservation. However, Hill *et al.* (2019) showed that even without those stresses, some reduction in zonal winds can be found in an axisymmetric model due to the finite width of the Hadley Cell updraft and turbulent mixing.

In an aqua-planet model with no longitudinal variation in the boundary conditions, $\alpha_\lambda = 1$ and so for the correct magnitude of the STJ, convection must occur at each longitude about $\alpha_t = 0.3$ of the time.

The transient motions involved in the Hadley Cell have both ISO and synoptic time-scales. The contributions to the JJA Hadley Cell are dominated by those from the Indian Ocean-west Pacific sector. This sector seems to split naturally into two, a South Asian/IO sector and a Philippines/WP sector. In both the ISO is strong, and the Hadley Cell extreme contributions come from times at which westward-moving waves enhance convection which is associated with a favourable phase of the ISO. These westward-moving waves have been identified with the WMRG waves coupled with convection analysed by Yang *et al.* (2007a; 2007b; 2007c).

In the upper troposphere, filaments of near-equatorial air move southwestwards into the SH. Some may turn cyclonically and return to the equatorial region. Others may be mixed in with the ambient SH air. However, in the big convective events they can reach the latitude of the STJ, and seemingly enhance both the magnitude of the STJ, the waves on it, and the transient momentum flux associated with them. In the lower troposphere, there is a suggestion that SH air feeding the NH convection comes from much deeper in the SH and around enhanced anticyclones there. In any case, it is clear that there is a strong extratropical–tropical interaction in these events, and that there is a strong two-way interaction between the Hadley Cell and the STJ, including the eddies on it.

Several questions follow from the analysis described here:

1. How well does the ERA-Interim dataset represent the detailed behaviour in the upper branch of the Hadley Cell?
2. How well is the behaviour represented in weather and climate models?
3. Are the details of the flow that average to give the Hadley Cell important?

The particular focus in Questions 1 and 2 is on the filamentary structure of the upper tropospheric air flowing from the summer hemisphere into the winter hemisphere, and sometimes as far as the STJ and interacting with it. Figure 14 does not indicate PV conservation in such filaments, but it does indicate only a slow change of the values with displacement from their origin. These filaments are relatively narrow in the horizontal, and also likely to be shallow in the vertical. The ERA-Interim analysis gives a striking and convincing view of the detailed behaviour in the upper branch of the Hadley Cell. However, it is possible that the analysis acts to smooth the PV in the region of such shallow, filamentary PV structures. Similarly, weather and climate models may need to have high horizontal and vertical resolution to represent them properly. In these models, the problem may be compounded by explicit or implicit mixing, particularly in the vertical direction. A further problem in modelling is that the filaments occur at the level of outflow from convective events in the summer Tropics. If this level is wrong or the sporadic nature of the convection is not well represented, then the behaviour will be wrong.

In two aspects, the answer to Question 3 must be yes. In the chemical composition of the atmosphere, the fact that the transport of upper tropospheric air from the summer to the winter hemisphere occurs in spasmodic, almost undiluted filaments rather than in the smooth manner suggested by the classic Hadley Cell picture must be highly significant in terms of the chemical reactions that take place.

Much of the discussion here has been about tropical weather and in particular the localised flaring of convection in tropical systems associated with the ISO and synoptic, WMRG waves. This is clearly important in tropical weather forecasting. The interaction of the upper-tropospheric tropical filaments with the STJ and the possible enhancement of the eddies on that jet means that the interaction may be important for extratropical weather and its prediction. There is also an intriguing hint that the low-level inflow to the enhanced tropical convection comes from deep in the SH.

Taking the view that climate is the ensemble of weather and given that the answer to Question 3 for weather has been yes, then it must also be yes in the case of climate. However, in other respects, whether the detailed behaviour that averages to give the Hadley Cell matters in climate is not as obvious. The large-scale constraints given by energetic and angular momentum consistency, as highlighted in, for example, the Held and Hou approach and discussed in Hill *et al.* (2019), may suggest that the details discussed here do not matter to first order. However, the important transfers of angular momentum by systems of tropical origin and the strong interaction of tropical upper-tropospheric filaments with the STJ suggest that it is indeed likely that they matter to first order.

In a subsequent article, the detailed structure of the Hadley Cell in the other solstitial season, December to February, will be analysed. It will be shown that the general conclusions drawn from the June to August season are again valid. However, there are new features associated with the ITCZ regions remaining north of the Equator, and with the occurrence of upper-tropospheric westerlies across much of the Pacific and Atlantic Ocean regions that will be highlighted.

ACKNOWLEDGEMENTS

The very helpful reviews by Spencer Hill and an anonymous reviewer have helped us to produce a much-improved article. BJH would like to acknowledge the many stimulating conversations he has had with Mike Blackburn that have helped him to develop the ideas behind the research discussed in this article. GYY acknowledges the long-term support of the National Centre for Atmospheric Science (NCAS), the NERC collaborative centre.

ORCID

G.-Y. Yang https://orcid.org/0000-0001-7450-3477
R. M. Fonseca https://orcid.org/0000-0002-8562-7368

REFERENCES

Dee, D.P., Uppala, S.M., Simmons, A.J., Berrisford, P., Poli, P., Kobayashi, S., Andrae, U., Balmaseda, M.A., Balsamo, G., Bauer, P., Bechtold, P., Beljaars, A.C.M., van de Berg, L., Bidlot, J., Bormann, N., Delsol, C., Dragani, R., Fuentes, M., Geer, A.J., Haimberger, L., Healy, S.B., Hersbach, H., Hólm, E.V., Isaksen, L., Kållberg, P., Köhler, M., Matricardi, M., McNally, A.P., Monge-Sanz, B.M., Morcrette, J.-J., Park, B.-K., Peubey, C., de Rosnay, P., Tavolato, C., Thépaut, J.-N. and Vitart, F. (2011) The ERA-interim reanalysis: configuration and performance of the data assimilation system. *Quarterly Journal of the Royal Meteorological Society*, 137, 553–597.

Dima, I.M. and Wallace, J.M. (2003) On the seasonality of the Hadley cell. *Journal of the Atmospheric Sciences*, 60, 1522–1527.

Emanuel, K.A. (1995) On thermally direct circulations in moist atmospheres. *Journal of the Atmospheric Sciences*, 52(9), 1529–1534. https://doi.org/10.1175/1520-0469(1995)052<1529:OTDCIM>2.0.CO;2.

Held, I.M. (2000) The general circulation of the atmosphere. In: *Proceedings of the Program in Geophysical Fluid Dynamics*. Woods Hole, MA: Woods Hole Oceanographic Institution. http://gfd.whoi.edu/proceedings/2000/PDFvol2000.html.

Held, I.M. and Hou, A.Y. (1980) Nonlinear axially symmetric circulations in a nearly inviscid atmosphere. *Journal of the Atmospheric Sciences*, 37(3), 515–533.

Hill, S.A., Bordoni, S. and Mitchell, J.L. (2019) Axisymmetric constraints on cross-equatorial Hadley cell extent. *Journal of the Atmospheric Sciences*, 76(6), 1547–1564. https://doi.org/10.1175/JAS-D-18-0306.1.

Hoskins, B.J. (1991) Towards a PV-θ view of the general circulation. *Tellus*, 43A, 27–36.

Hoskins, B.J., McIntyre, M.E. and Robertson, A.W. (1985) On the use and significance of isentropic potential vorticity maps. *Quarterly Journal of the Royal Meteorological Society*, 111, 877–946.

Jeffreys, H. (1926) On the dynamics of the geostrophic winds. *Quarterly Journal of the Royal Meteorological Society*, 52(217), 85–104.

Lee, S.-S. and Wang, B. (2016) Regional boreal summer intraseasonal oscillation over Indian Ocean and western Pacific: comparison and predictability study. *Climate Dynamics*, 46, 2213–2229. https://doi.org/10.1007/s00382-015-2698-7.

Liebmann, B. and Smith, C.A. (1996) Description of a complete (interpolated) outgoing longwave radiation dataset. *Bulletin of the American Meteorological Society*, 77, 1275–1277.

Lindzen, R.S. and Hou, A.V. (1988) Hadley circulations for zonally averaged heating centered off the Equator. *Journal of the Atmospheric Sciences*, 45(17), 2416–2427.

Lorenz, E.N. (1967) *The Nature and Theory of the General Circulation of the Atmosphere*, Vol. 218. Geneva: World Meteorological Organization Publications, p. 161.

Paldor, N. and Killworth, P.D. (1988) Inertial trajectories on a rotating Earth. *Journal of the Atmospheric Sciences*, 45, 4013–4019.

Plumb, R.A. and Hou, A.Y. (1992) The response of a zonally symmetric atmosphere to subtropical thermal forcing: threshold behavior. *Journal of the Atmospheric Sciences*, 49, 1790–1799.

Rodwell, M.R. and Hoskins, B.J. (1995) A model of the Asian summer monsoon. II: Cross-equatorial flow and PV behaviour. *Journal of the Atmospheric Sciences*, 52, 1341–1356.

Schneider, E.K. (1977) Axially symmetric steady-state models of the basic state for instability and climate studies. Part II: Nonlinear calculations. *Journal of the Atmospheric Sciences*, 34(2), 280–296.

Schneider, T. (2006) The general circulation of the atmosphere. *Reviews of Earth and Planetary Science*, 34, 655–688.

Tomas, R.A. and Webster, P.J. (1997) The role of inertial instability in determining the location and strength of near-equatorial convection. *Quarterly Journal of the Royal Meteorological Society*, 123(542), 1445–1482. https://doi.org/10.1002/qj.49712354202.

Wang, B. and Rui, H. (1990) Synoptic climatology of transient tropical intra-seasonal convection anomalies. *Meteorology and Atmospheric Physics*, 44, 43–61.

Yang, G.-Y., Hoskins, B.J. and Slingo, J.M. (2007a) Convectively coupled equatorial waves. Part I: Horizontal structure. *Journal of the Atmospheric Sciences*, 64, 3406–3423.

Yang, G.-Y., Hoskins, B.J. and Slingo, J.M. (2007b) Convectively coupled equatorial waves. Part II: Zonal propagation. *Journal of the Atmospheric Sciences*, 64, 3424–3437.

Yang, G.-Y., Hoskins, B.J. and Slingo, J.M. (2007c) Convectively coupled equatorial waves. Part III: Synthesis structures and extratropical forcing. *Journal of the Atmospheric Sciences*, 64, 3438–3451.

Yang, G.-Y., Methven, J., Woolnough, S.J., Hodges, K. and Hoskins, B.J. (2018) Linking African easterly wave activity with equatorial waves and the influence of Rossby waves from the Southern Hemisphere. *Journal of the Atmospheric Sciences*, 75, 1783–1809.

Zhuang, M. and Duan, A. (2019) Revisiting the cross-equatorial flows and Asian summer monsoon precipitation associated with the Maritime Continent. *Journal of Climate*, 32, 6803–6821.

SUPPORTING INFORMATION

Additional supporting information may be found online in the Supporting Information section at the end of this article.

How to cite this article: Hoskins BJ, Yang G-Y, Fonseca RM. The detailed dynamics of the June–August Hadley Cell. *Q J R Meteorol Soc*. 2020;1–19. https://doi.org/10.1002/qj.3702

APPENDIX

Some equations used in the text

It is convenient to use $\mu = \sin\phi$ as latitudinal coordinate, where ϕ is the latitude, and $U = u\cos\phi$, $V = v\cos\phi$ as velocity variables. The specific absolute angular momentum is

$$A = a^2\Omega(1-\mu^2) + aU, \tag{A1}$$

where a is the radius of the Earth, and Ω its rotation rate.

The vertical component of absolute vorticity is

$$\zeta = 2\Omega\mu + \frac{1}{a(1-\mu^2)}\frac{\partial V}{\partial\lambda} - \frac{1}{a}\frac{\partial U}{\partial\mu}. \tag{A2}$$

The potential vorticity (PV) is

$$P = \frac{1}{\rho}\boldsymbol{\zeta}\cdot\boldsymbol{\nabla}\theta, \tag{A3}$$

where $\boldsymbol{\zeta}$ is the 3-D absolute vorticity. On large length-scales, the term corresponding to the vertical component of $\boldsymbol{\zeta}$ dominates, and

$$P \approx \frac{1}{\rho}\zeta\frac{\partial\theta}{\partial z}. \tag{A4}$$

In the Tropics the stratification varies little in the horizontal and in time, so that

$$P \approx \frac{1}{\rho}\zeta\frac{d\theta_r}{dz}, \tag{A5}$$

where $\theta_r(z)$ is a reference stratification.

From Equation A1,

$$\frac{1}{a}\frac{\partial A}{\partial\mu} = -a\zeta + \frac{1}{1-\mu^2}\frac{\partial V}{\partial\lambda}. \tag{A6}$$

Therefore, in a zonal average, denoted by [],

$$\frac{1}{a}\frac{\partial[A]}{\partial\mu} = -a[\zeta]. \tag{A7}$$

The equation for the material rate of change of A is, in pressure coordinates,

$$\frac{DA}{Dt} = -\frac{\partial\Phi}{\partial\lambda} + F, \tag{A8}$$

where $\frac{D}{Dt} = \frac{\partial}{\partial t} + \frac{1}{a(1-\mu^2)}U\frac{\partial}{\partial\lambda} + \frac{1}{a}V\frac{\partial}{\partial\mu} + \omega\frac{\partial}{\partial p}$, Φ is the geopotential and F is the frictional torque.

In flux form,

$$\frac{\partial A}{\partial t} = -\frac{1}{a(1-\mu^2)}\frac{\partial}{\partial\lambda}(UA) - \frac{1}{a}\frac{\partial}{\partial\mu}(VA) - \frac{\partial}{\partial p}(\omega A) - \frac{\partial\Phi}{\partial\lambda} + F. \tag{A9}$$

In the zonal average and using U instead of A in the fluxes,

$$\frac{\partial[A]}{\partial t} = a\frac{\partial[U]}{\partial t} = -\frac{\partial}{\partial\mu}[UV] - a\frac{\partial}{\partial p}[\omega U] - af[V] + [F]. \tag{A10}$$

An alternative form emphasising the role of the absolute vorticity flux is:

$$\frac{\partial [A]}{\partial t} = a\frac{\partial [U]}{\partial t} = a[V\zeta] - a\left[\omega\frac{\partial U}{\partial p}\right] + [F]. \quad \text{(A11)}$$

For the vertical component of absolute vorticity,

$$\frac{D\zeta}{Dt} = \zeta\frac{\partial \omega}{\partial p} - \boldsymbol{k}\cdot\left(\boldsymbol{\nabla}\,\omega \times \frac{\partial \boldsymbol{V}}{\partial p}\right) + a\boldsymbol{k}\cdot(\boldsymbol{\nabla}\times\boldsymbol{F}), \quad \text{(A12)}$$

where $\boldsymbol{V} = (U, V)$ and $\boldsymbol{F}/a$ is the friction in the equation for $\boldsymbol{V}$. Here the twisting term, the second term on the right-hand side will be small on large scales. In the zonal average, the flux form, which can also be derived by taking $a^{-2}\partial/\partial\mu$ of Equation A11, is:

$$\frac{\partial [\zeta]}{\partial t} = -a\frac{\partial}{\partial \mu}[V\zeta] + \frac{1}{a}\frac{\partial}{\partial \mu}\left[\omega\frac{\partial U}{\partial p}\right] - \frac{1}{a^2}\frac{\partial}{\partial \mu}[F]. \quad \text{(A13)}$$

The material rate of change of PV is

$$\frac{DP}{Dt} = \frac{1}{\rho}\{\boldsymbol{\zeta}\cdot\boldsymbol{\nabla}\,\dot{\theta} + a(\boldsymbol{\nabla}\times\boldsymbol{F})\cdot\boldsymbol{\nabla}\,\theta\}. \quad \text{(A14)}$$